Tagging moisture sources with Eulerian and Lagrangian tracers:Application to an intense atmospheric river event

Vicente Pérez-Muñuzuri[1*], Jorge Eiras-Barca[1], Daniel Garaboa-Paz[1], and Gonzalo Míguez-Macho[1]

Published: 08/11/2017
Academic Editor: Francina Dominguez

[1] Group of Nonlinear Physics. Faculty of Physics. University of Santiago de Compostela. 15782 Santiago de Compostela, Spain.
* Correspondence: vicente.perez@cesga.es

Abstract: One Eulerian and two Lagrangian tracers tools are evaluated for studies on atmospheric moisture sources and pathways. The first method has been recently implemented into the Weather Research and Forecasting (WRF) mesoscale model, while the Lagrangian methods are described here. In these methods, a moisture volume is assigned to each particle, which is then advected by the wind flow. Usual Lagrangian methods consider this volume to remain constant and the particle follows flow path lines exactly. In a different approach,, the initial moisture volume can be considered to depend on time as it's advected by the flow, due to thermodynamic processes. In this case, the tracer volume drag must be taken into account. Equations have been implemented and moisture convection was represented in both Lagrangian models. We apply these methods to evaluate the intense atmospheric river that devastated the Pacific North West region of the United States, with flooding rains and intense winds in early November 2006. We note that the usual Lagrangian method underestimates moisture availability in the continent while active tracers (both Eulerian and Lagrangian) achieve more realistic results.

Keywords: active tracers, eulerian, lagrangian, atmospheric rivers.

1. Introduction

Extreme precipitation and flooding in many areas of the world, and particularly on the US and Europe west coasts, are often related to the presence of atmospheric rivers (ARs) [3, 25, 14, 4]. ARs are narrow and elongated filamentous structures that transport moisture from the tropics into mid-latitudes over a period of a few days, and usually form in association with baroclinic systems. AR conditions occur in the warm sector of extratropical cyclones and are characterized by large water vapor contents and transport at low levels [24]. For some AR events, a filamentous pattern develops persisting enough time to be considered a Lagrangian coherent structure [8, 9]. ARs have been shown to play a key role in extratropical tropospheric dynamics [20, 33, 12]. The advection and convergence of moisture along ARs is a key process for Earth's sensible and latent heat redistribution and has a strong impact on the mid-latitudes water cycle by increasing tropospheric water vapor mixing [33].

The present study examines a uniquely well-observed extreme precipitation event to better understand the role of the landfalling AR that devastated portions of the US Pacific Northwest coast with torrential rains and severe flooding on 6-7 November 2006 [19]. The composite analysis of the

vertically integrated water vapor transport (IVT) and the integrated column of water vapor (IWV) (Fig. 1) provides a depiction of the landfalling AR during its most destructive phase. The figure shows a narrow plume extending northeastward from the tropical moisture reservoir to the Pacific Northwest, and strongly suggests direct incorporation of tropical moisture into the AR. The landfalling AR was observed to occur on 6th November and led to important precipitation amounts (Fig. 2) in the northwestern coast of North America. In addition, these images also show the development of a very deep depression, which in conjunction with an anticyclone located to the southeast, increases the poleward and eastward flux of moisture with an apparent tropical origin.
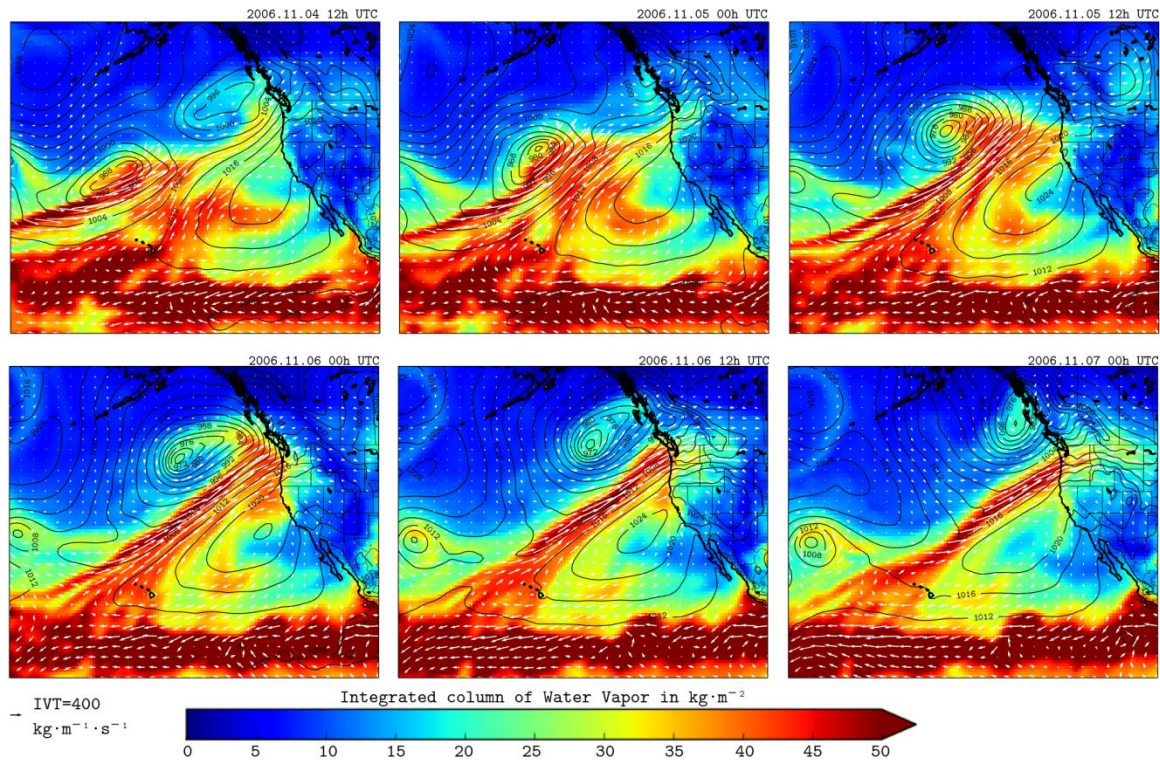
Figure 1. Composite analysis of the vertically integrated horizontal water vapor transport (IVT, kg m^{-1} s^{-1}) and the integrated column of water vapor (IWV, kg m^{-2}) derived from the ERA-Interim daily reanalysis dataset for 4-7 Nov 2006.

To analyze the contribution of tropical moisture onto the landfalling ARs different numerical methods have been applied in the last decades, namely analytical, Lagrangian and Eulerian models (e.g. [11], for a detailed review). Lagrangian models have been widely used in climatic studies of atmospheric water vapor sources and in the diagnosis of the origin of moisture in extreme precipitation events [28, 29, 10, 26]. These models, although widely used, cannot describe correctly evaporation (e) and precipitation (p), in addition to neglecting liquid water and ice, which results in an overestimation of both e and p. All Lagrangian models consider constant parcel volumes. However, the initial parcel may change its volume along its pathway due to thermodynamic and mechanical effects. In this case, inertial effects on the parcel should be considered [17]. Finite-size or inertial particle dynamics in fluid flows can differ markedly from Lagrangian particle dynamics, in both, their motion and clustering behavior (e.g. [18], for a review). Eulerian methods, generally known as water vapor tracers (WVTs) are based on coupling a moisture tagging technique with a global or regional meteorological model [27, 13, 5]. This strategy allows the model to explicity account for all physical processes affecting atmospheric moisture, but on the other hand, it cannot be run offline and thus cannot be coupled to an atmospheric reanalysis, for example. This paper presents a comparison between Eulerian and Lagrangian methods for the landfalling AR episode on November

2016. Two Lagrangian models will be considered depending on wheter inertial forces on tracers are considered or not.
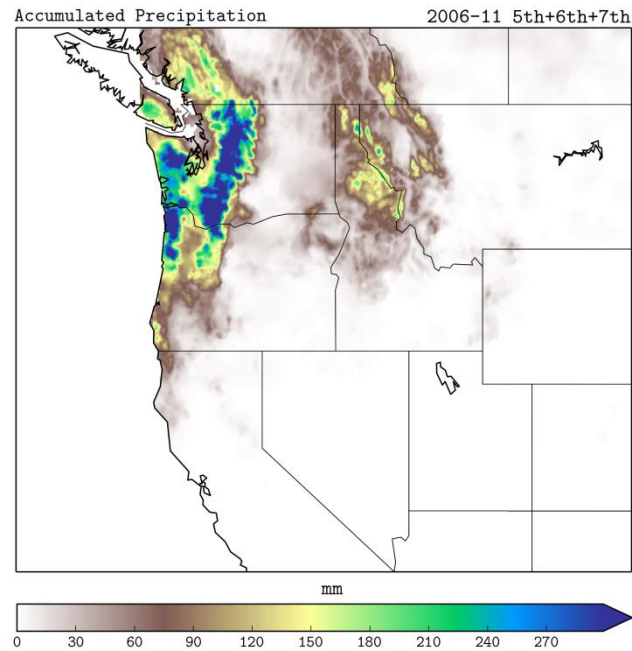
Figure 2. Accumulated precipitation for 5-7 Nov 2006. Precipitation datasets were obtained from [15].

2. Model

2.1. Eulerian tracer model

The Eulerian tracer model is based on coupling a moisture tagging technique with the WRF model. The prognostic equations for the different moisture species are replicated with equations for moisture tracers, which are defined as moisture originating from a predetermined source. In the equations for tracers, turbulent diffusion uses the same eddy diffusivities as for full moisture, and convection and microphysics processes for tracers follow those for full moisture, assuming that phase changes among the different tracer species occur in amounts proportional to the tracer fraction in the species undergoing the change. The tracer tool can separate moisture from different sources with a very small error (less than 1% in traceability). The uncertainty of the method is almost entirely due to the WRF model errors. A more in-depth description of the Eulerian tracer tool and validation results can be found in in [5] and in [13].

For the numerical experiments, all moisture contained below latitudes 25/28 (considering the WRF lambert conformal projection grid conversion to lat-lon) is labeled and tracked in its path northward. Advection, convection and change of phase of this tagged moisture along the way are solved and considered by WRF. Figure 3 shows the complete domain of simulation highlighted in both blue and red areas. The red area depicts tropical latitudes, where moisture is initially tagged.
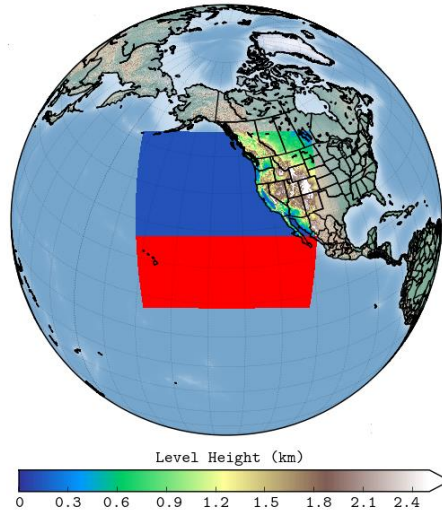
Figure 3. Simulation domain (red+blue) used in the WRF tracers tool. Red area matches the tropical latitudes where the moisture is initially tagged.

2.2. Inertial and Lagrangian models

The atmospheric transport has been studied using wind field data obtained from the European Center for Medium-Range Weather Forecast reanalysis, ERA-Interim [2]. The spatial resolution of the data set is approximately 80 km (T255 spectral) on 60 vertical levels from the surface up to 0.1 hPa, and a temporal resolution of 6 hours. Datasets were retrieved in a longitudelatitude-height coordinate system (φ, θ, z) on model levels.

Two types of fluid particles have been considered in this study; inertial and Lagrangian particles. In the first case, the particles' volume are assumed to change with time, while Lagrangian particles keep their volume constant. A Lagrangian particle is then advected using the trajectory equation

$$\frac{dx_i}{dt} = u_i[x_i(t), t] \tag{1}$$

where *i* is the i-component of the fluid velocity, and u_i is the wind velocity interpolated in space and time from an external source at the particles' position x_i. Thus, Lagrangian particles follow wind stream trajectories However, inertial tracers accelerate due to external forces acting on the particle and their motion in non-uniform incompressible flows can be modeled by the momentum equation [32, 18, 31, 21],

$$\frac{dv_i}{dt} = \frac{Du_i}{Dt} + 2\Omega \times U_i + C_L(U_i \times \omega_i) + \frac{9\upsilon}{R^2}U_i + \frac{1}{2R^3}\left(\frac{d(R^3 U_i)}{dt} + 2R^3\frac{dU_i}{dt}\right) \tag{2}$$
$$- \frac{9}{2R^3}\sqrt{\frac{\overline{\upsilon}}{\pi}} \int_{-\infty}^{t} \frac{1}{\sqrt{\int_{\tau}^{t'} R^{-2} dt'}} \frac{d(RU_i)}{d\tau} d\tau$$

where v_i is the velocity of the inertial tracer, u_i that of the fluid, $U_i = u_i - v_i$ the relative velocity between the fluid and the tracer, ω_i the fluid vorticity, $C_L = 0.5$ the lift coefficient for a sphere, ρ the air density, $\nu = \mu/\rho$,the kinematic viscosity, and Ω the Earth angular velocity. The six terms on the right represent, respectively, the force exerted by the undisturbed flow, the Coriolis force, the lift force, the Stokes drag, the viscous force, and the history force. In the last two terms, the effect of a spherical tracer with a time-dependent radius $R(t)$ has been considered [16, 31]. The derivative D/Dt is taken along the path of a fluid element, whereas the derivative d/dt is taken along the trajectory of the particle.

The instantaneous parcel radius R(t) is calculated from the Rayleigh–Plesset equation [22] of parcel dynamics

$$R\frac{d^2R}{dt^2} + \frac{3}{2}\left(\frac{dR}{dt}\right)^2 = \frac{P_f - P}{\rho} \tag{3}$$

Further generalizations of this equation to a compressible fluid [23] have been published, but for the purpose of this study we will keep a first order approach, since the flow is mainly driven by the momentum equation (2). In Eq. (3), dR/dt and d^2R/dt^2 are the parcel wall velocity and acceleration, respectively, P_f is the pressure in the fluid at the parcel interface,and P is the pressure field imposed by the flow. The pressure at the parcel interface is given by,

$$P_f(R) = P_v + P_g - \frac{2\gamma}{R} - \frac{4\mu}{R}\frac{dR}{dt} \tag{4}$$

in which the first two terms are the internal pressure of the parcel related to the partial pressure due to vapor content P_v and gas content P_g, respectively, and the last terms account for the interface curvature effect and the viscous stress at the interface. Surface tension is given by γ and for our simulations, it can be considered negligible $\gamma \sim 0$. The gas pressure inside the parcel changes as the parcel contracts or expands. As the total amount of gas in the tracer remains constant, the tracer radius and gas pressure are related by $P_g = P_{g0}(R/R_0)^{3\alpha}$, where $\alpha = 1$ for an isothermal process, or equal to the ratio of specific heats for an adiabatic process. The external P and vapor pressures are interpolated in space and time from the meteorological model at the particle position.

Updrafts and downdrafts due to moist convection were considered for both models. To represent convective transport in a particle dispersion model, it is necessary to redistribute particles in the entire vertical column as these transports are not represented by the ERA-Interim vertical velocity. Here, we follow the same convective parameterization implemented in the Lagrangian dispersion model FLEXPART [6, 30].

For the numerical experiments, a regular grid of $N = 60 \times 34$ particles is homogeneously distributed in the interval $(\theta, \varphi) \in [160W, 110W] \times [7N, 25N]$ and for 30 vertical levels from the surface up to 5 km above the ground. Then, 3D Lagrangian simulations have been performed so that particle trajectories are computed integrating equations above using a 4th order Runge-Kutta scheme with a fixed time step of $\Delta t = 1$ s, and multilinear interpolation in time and space from current 60-level ECMWF data. Particles are advected during 60 hours beginning the 5th November 2006 at 0h UTC and every 6 hours a new grid of particles is released from the original location. The history term in Eq. (2) is integrated following the numerical integration scheme depicted by [1].

To study the trajectory followed by a tagged mass of vapor, an initial volume of radius $R_0 = 50$ m and specific humidity q_v^t is assigned to each inertial/Lagrangian particle. The net change of water vapor content is given by,

$$e - p = \frac{d(mq_v^t)}{dt} \tag{5}$$

where m is the mass of a particle, and $e - p$ measures the net excess or shortage of water vapor at the particle position. For the inertial tracers, the volume of the particle changes with time, while m is constant for the Lagrangian particles. At any time, we assume that water vapor and temperature of the particles are equal to the surrounding values interpolated from ERA-Interim at the particle position $q_v^{part}(t) = q_v(t)$. Besides, the water vapor content inside the particle is equal to the tagged humidity plus some moisture up to q_v, $q_v^{part}(t) = q_v^t(t) + q_v^r(t)$ for $t = 0$, $q_v^{part}(t = 0) = q_v^t(t = 0)$ and $q_v^r(t = 0) = 0$. Integration of Eq. (5) results in a decrease of the tagged moisture only when the water vapor excess $\varepsilon = q_v(t - \Delta t) - q_v(t)$ is positive,

$$q_v^t(t) = q_v^t(t - \Delta t) - \frac{\epsilon \Delta t}{m}\left(\frac{q_v^t(t - \Delta t)}{q_v(t - \Delta t)}\right) \tag{6}$$

where $m = \rho V(t)$ for an inertial particle, and the last term represents the percentage of moisture reduction ε for the tagged water vapor. Otherwise, if $\varepsilon \leq 0$ the tagged moisture does not change.

3. Results

Tagged moisture advected from the Tropics and simulated with the Eulerian model is shown in Fig. 4. The integrated water vapor shows and intense plume of moisture extending from the tropical water vapor reservoir to Washington and Oregon as it was shown in the reanalysis, Fig. 1. Landfalling of the AR occurs the 6th of November at 0h UTC. During the next hours moisture continues to reach the continent while displacing to the south and reaching Northern California.3.1.

Inertial and Lagrangian tagged tracers also reproduce the trajectory of the AR (Figs 5-6). Unlike the Eulerian model, these tracers are initially trapped by the vortical structure of the depression located northward of the AR that drags them while moving toward the northeast (see Fig. 1 for a time sequence). Compared to Lagrangian particles, heavier inertial particles loaded with moisture are observed around the depression. Later on, 36h after being initialized, tagged inertial particles can be observed inland north of Montana, while this is not the case for the Lagrangian tracers. Note that IVT images show also some moisture at the same location. However, the cloud of inertial particles extend inland as time goes on (48h) and it does not decrease either in extension or in mean value, in contrast with what happens for Lagrangian and Eulerian tracers. In this case, the known moisture overestimation excedes   for the Lagrangian models, since Eq. (6), does not favor the elimination of moisture above the ground. On November 7th, inertial and eulearian tracers reach northern California favored by the northward turn of the low, as observed in the IVT analysis, but this does not occur for the Lagrangian ones. The extreme nature of the November 2006 precipitation event (Fig

2) is reflected in the extreme values of the tagged moisture content over the North Pacific coast.
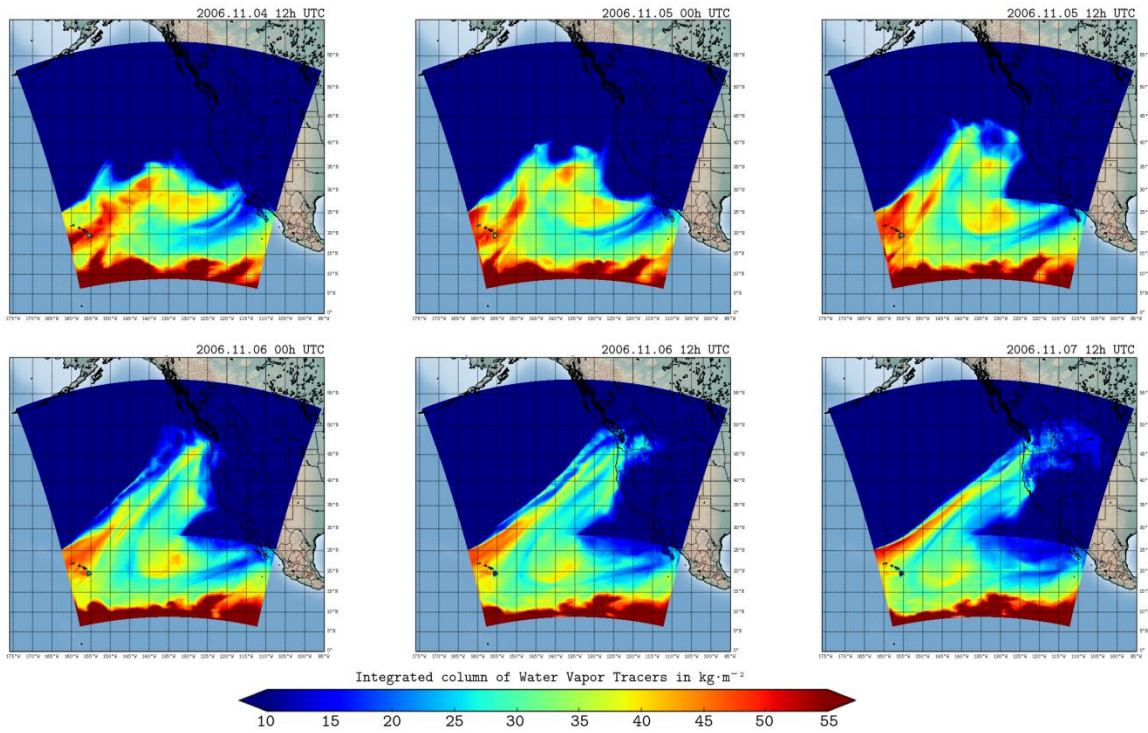
Figure 4. Vertically integrated tagged water vapor from the Tropics obtained from the Eulerian model.
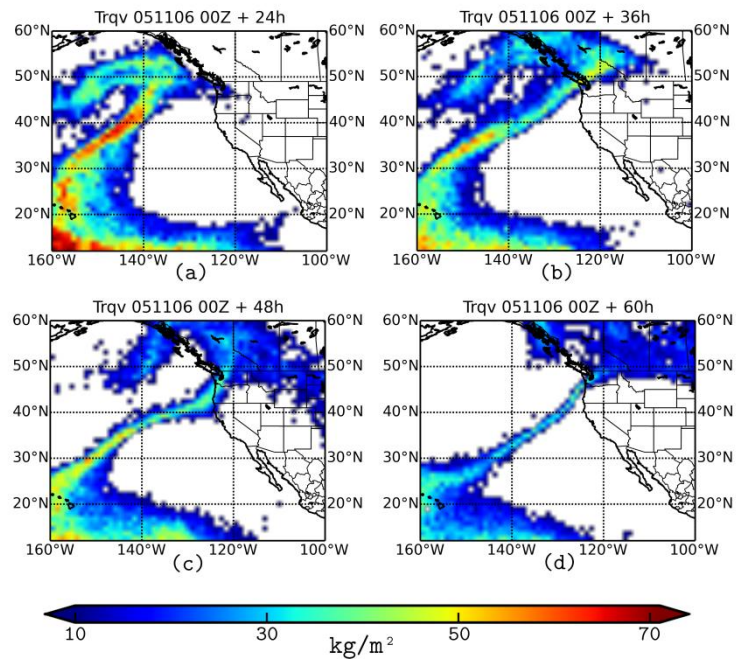
Figure 5. Vertically integrated tagged water vapor from the Tropics obtained from the inertial model.
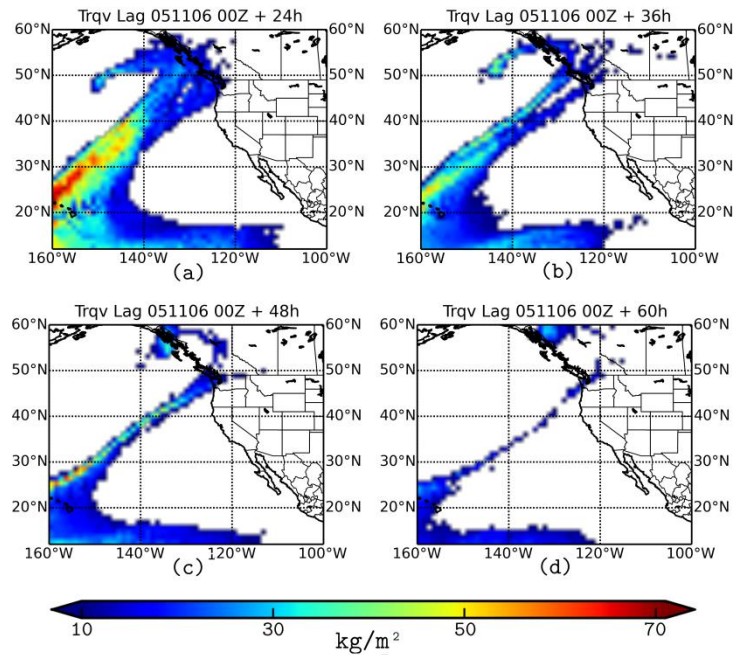
Figure 6. Vertically integrated tagged water vapor from the Tropics obtained from the Lagrangian
model.

Figure 7 resumes the behavior of both inertial and Lagrangian moisture contents over three sites located in the coast of Washington, Oregon and North California states, respectively. As mentioned above, the tagged vapor content of the inertial tracers rapidly increases as the AR approaches Washington, but the maximum is delayed as it moves to the south; Oregon and North California. However, although the Lagrangian particles show different average moisture contents for the three sites, the impact of the landfalling AR is smoothed if compared to the inertial ones.
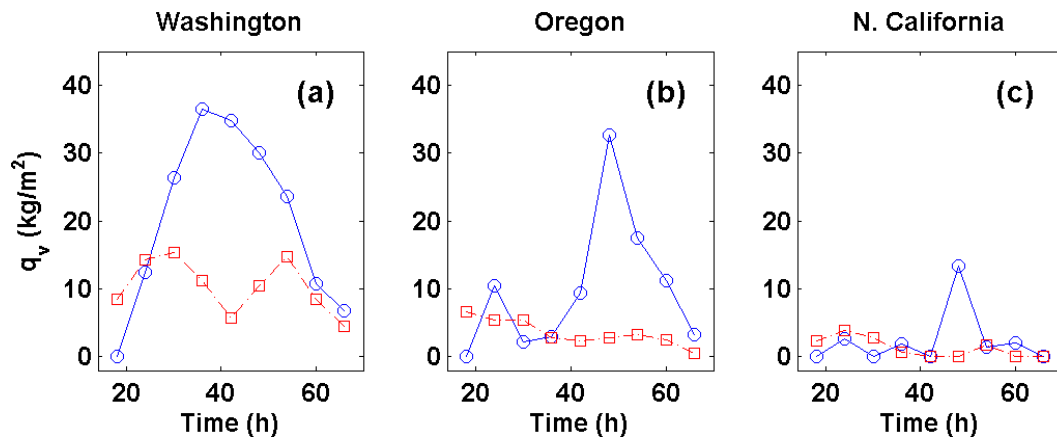
Figure 7. Time evolution of the tagged vertically integrated moisture concentration for three sites in the northeastern coast of US. Inertial (dots) and Lagrangian (squares) tracers.

4. Conclusions

Three Eulerian, Lagrangian and inertial models have been used to compare the trajectories of tagged moisture from the Tropics to evaluate the intense atmospheric river that devastated the US Pacific North West with flooding rains and intense winds in early November 2006. The three models reproduce the structure of the AR. Inertial and Lagrangian tracers are dragged northeastward by the low while Eulerian tracers reproduce better the landfalling of the AR. Tagged inertial moisture concentrations over the coast are larger than Lagrangian ones, and they reach Northern California as the low turns to the north.

Further improvements on both Lagrangian and inertial models should be undertaken to correct the vapor excess above the ground. The presence of larger moisture amounts around the low not reproduced by the Eulerian model is likely related to the lack of precipitation in Lagrangian and active formalisms. The influence of the initial tracer deployment should also be studied in detail. Particle models were initialized several days later than the Eulerian model, and hence were able to influence the width of the river and its motion southward.

These results highlight the important contribution of tropical moisture to atmospheric rivers and the different dynamical behaviors reproduced by the three models considered here. However, an in-depth investigation with a sufficient number of cases and further diagnostics would be needed to draw a more robust general conclusion.

Conflicts of Interest: The authors declare that they have no conflict of interest.

References

[1] Daitche, A. Advection of inertial particles in the presence of the history force: Higher order numerical schemes. J. Comp Phys., 254, 93–106, doi:10.1016/j.jcp.2013.07.024, 2013.

[2] Dee, D.P., S. M. Uppala, A.J. Simmons, P. Berrisford, P. Poli, S. Kobayashi, U. Andrae, M. A. Balmaseda, G. Balsamo, P. Bauer, P. Bechtold, A. C. M. Beljaars, L. van de Berg, J. Bidlot, N. Bormann, C. Delsol, R. Dragani, M. Fuentes, A.J. Geer, L. Haimberger, S. B. Healy, H. Hersbach, E. V. Holm, L. Isaksen, P. Kallberg, M. Koehler, M. Matricardi, A. P. McNally, B. M. Monge-Sanz, J.J. Morcrette, B.K. Park, C. Peubey, P. de Rosnay, C. Tavolato, J.N. Thepaut, and F. Vitart. The ERA-Interim reanalysis: configuration and performance of the data assimilation system, Q. J. Roy. Meteo. Soc., 137, 553–597, doi:10.1002 qj.828, 2011.

[3] Dettinger, M.D., F.M. Ralph, T. Das, P.J. Neiman, and D.R. Cayan. Atmospheric rivers, floods and the water resources of California. Water, 3(2), 445–478, 2011.

[4] Eiras-Barca, J., S. Brands, and G. Míguez-Macho. Seasonal variations in North Atlantic atmospheric river activity and associations with anomalous precipitation over the Iberian Atlantic Margin. Journal of Geophysical Research: Atmospheres. 21(2), 931–948, doi:10.1002/2015JD023379, 2016.

[5] Eiras-Barca, J., Dominguez, F., Hu, H., Garaboa-Paz, A. D., and Miguez-Macho, G.: Evaluation of the Moisture Sources in two Extreme Landfalling Atmospheric River Events using an Eulerian WRF-Tracers tool, Earth System Dynamics Discussions, 2017, 1-21, doi:10.5194/esd-2017-63, 2017.

[6] Emanuel, K. A., and Zivkovic-Rothman, M. Development and evaluation of a convection scheme for use in climate models. J. Atmos. Sci., 56, 1766–1782, 1999.

[7] Forster, C., Stohl, A., and Seibert, P., Parameterization of convective transport in a Lagrangian particle dispersion model and its evaluation. J. Appl. Meteor. Climatol., 46, 403–422, doi:10.1175/JAM2470.1, 2007.

[8] Garaboa-Paz, D., J. Eiras-Barca, F. Huhn, and V. Pérez-Muñuzuri. Lagrangian coherent structures along atmospheric rivers, Chaos, 25(6), 063105, doi:10.1063/1.4919768, 2015.

[9] Garaboa-Paz, D., J. Eiras-Barca, and V. Pérez-Muñuzuri. Climatology of Lyapunov exponents: the link between atmospheric rivers and large-scale mixing variability. Earth Syst. Dynam., 8, 865–873, doi:10.5194/esd-8-865-2017, 2017.

[10] Gimeno, L., Drumond, A., Nieto, R., Trigo, R. M., and Stohl, A. On the origin of continental precipitation, Geophysical Research Letters, 37, 1–7, doi:10.1029/2010GL043712, 2010.

[11] Gimeno, L., Stohl, A., Trigo, R. M., Dominguez, F., Yoshimura, K., Yu, L., Drumond, A., Durn-Quesada, A. M., and Nieto, R. Oceanic and terrestrial sources of continental precipitation, Reviews of Geophysics, 50, 1–41, doi:10.1029/2012RG000389, 2012.

[12] Gimeno, L., F. Dominguez, R. Nieto, R. Trigo, A. Drumond, C.J.C. Reason, A. Taschetto, A.M. Ramos, R. Kumar, and J. Marengo. Major Mechanisms of Atmospheric Moisture Transport and Their Role in Extreme Precipitation Events. Annual Review of Environment and Resources, 41(1), 117–141, doi:annurevenviron-110615-085558, 2016.

[13] Insua-Costa, D. and Miguez-Macho, G. A new moisture tagging capability in the Weather Research and Forecasting Model: formulation, validation and application to the 2014 Great Lake-effect snowstorm, Earth Syst. Dynam. Discuss., https://doi.org/10.5194/esd-2017-80, in review, 2017.

[14] Lavers, D.A., and G. Villarini. The nexus between atmospheric rivers and extreme precipitation across Europe. Geophysical Research Letters, 40(12), 3259–3264, doi:10.1002/grl.50636, 2013.

[15] Livneh, B., Bohn, T. J., Pierce, D.W., Munoz-Arriola, F., Nijssen, B., Vose, R., Cayan, D. R., and Brekke, L.: A spatially comprehensive, hydrometeorological data set for Mexico, the US, and Southern Canada 1950–2013, Scientific data, 2, 2015.

[16] Magnaudet, J. and Legendre, D. The viscous drag force on a spherical bubble with a time-dependent radius. Phys. Fluids, 10, 550–554, doi:10.1063/1.869582, 1998.

[17] Maxey, M.R. and Riley, J.J. Equation of motion for a small rigid sphere in a nonuniform flow. Phys. Fluids, 26, 883–889, doi:10.1063/1.864230, 1983

[18] Michaelides, E.E. Hydrodynamic force and heat/mass transfer from particles, bubbles, and drops. J. Fluids Eng. 125, 209–238, doi:10.1115/1.1537258, 2003.

[19] Neiman, P.J., Ralph, F.M.,Wick, G.A., Kuo, Y.,Wee, T., Ma, Z., Taylor, G.H., and Dettinger, M.D. Diagnosis of an Intense Atmospheric River Impacting the Pacific Northwest: Storm Summary and Offshore Vertical Structure Observed with COSMIC Satellite Retrievals. Mon. Wea. Rev., 136, 4398–4420, doi:10.1175/2008MWR2550.1, 2008.

[20] Newell, R.E., N.E. Newell, Y. Zhu, and C. Scott. Tropospheric rivers? A pilot study. Geophysical Research Letters, 19(24), 2401–2404, doi:10.1029/92GL02916, 1992.

[21] Pérez-Muñuzuri, V., and Garaboa-Paz, D. Mixing of spherical bubbles with time-dependent radius in incompressible flows, Phys. Rev. E, 93, 023107, doi:10.1103/PhysRevE.93.023107, 2016.

[22] Plesset, M.S., and Prosperetti, A. Bubble dynamics and cavitation. Ann. Rev. Fluid Mech., 9, 145–185, doi:10.1146/annurev.fl.09.010177.001045, 1977.

[23] Prosperetti, A. The equation of bubble dynamics in a compressible liquid. Phys. Fluids, 30, 3626–3628, doi:10.1063/1.866445, 1987.

[24] Ralph, F. M., P. J. Neiman, D. E. Kingsmill, P. O. G. Persson, A. B. White, E. T. Strem, E. D. Andrews, R. C. Antweiler, and G. A. Wick. Satellite and CALJET aircraft observations of atmospheric rivers over the eastern North Pacific Ocean during the winter of 1997/98. Mon. Wea. Rev., 132, 1721–1745, 2004.

[25] Ralph, F.M., and M.D. Dettinger. Storms, floods, and the science of atmospheric rivers. Eos T. Am. Geophys. Un., 92(32), 265–266, 2011.

[26] Ramos, A.M., Nieto, R., Tomé, R., Gimeno, L., Trigo, R.M., Liberato, M.L., and Lavers, D. A. Atmospheric rivers moisture sources from a Lagrangian perspective. Earth Syst. Dynam., 7, 371–384, doi:10.5194/esd-7-371-2016, 2016.

[27] Singh, H. A., Bitz, C. M., Nusbaumer, J., and Noone, D. C. A mathematical framework for analysis of water tracers: Part 1: Development of theory and application to the preindustrial mean state, Journal of Advances in Modeling Earth Systems, 8, 991–1013, 2016.

[28] Stohl, A. and James, P. A Lagrangian analysis of the atmospheric branch of the global water cycle. Part I: Method description, validation, and demonstration for the August 2002 flooding in Central Europe, Journal of Hydrometeorology, 5, 656–678, doi:10.1175/1525-7541(2004)005<0656:ALAOTA>2.0.CO;2, 2004.

[29] Stohl, A. and James, P. Lagrangian analysis of the atmospheric branch of the global water cycle. Part II: Moisture transports between Earths ocean basins and river catchments, Journal of Hydrometeorology, 6, 961–984, doi:10.1175/JHM470.1, 2005.

[30] Stohl, A., Forster, C., Frank, A., Seibert, P., and Wotawa G. Technical Note: The Lagrangian particle dispersion model FLEXPART version 6.2. Atmos. Chem. Phys. 5, 2461-2474, doi:10.5194/acp-5-2461-2005, 2005.

[31] Takemura, F., and Magnaudet, J. The history force on a rapidly shrinking bubble rising at finite Reynolds number. Phys. Fluids 16, 3247–3255, doi:10.1063/1.1760691, 2004.

[32] Zapryanov Z., and Tabakova, S. Dynamics of bubbles, drops and rigid particles (Science+Business Media Dordrecht, 1999).

[33] Zhu, Y., and Newell, R. A proposed algorithm for moisture fluxes from atmospheric rivers, Mon. Wea. Rev., 126, 725–735, doi:10.1175/1520-0493(1998)1263C0725:APAFMF3E2.0.CO;2, 1998.